Effect of hydrostatic pressure on the thermoelectric properties of Bi_2Te_3

Wilfredo Ibarra-Hernández,* Matthieu J. Verstraete, and Jean-Yves Raty
Département de Physique, Université de Liège, Allée du 6 Août 17, B-4000 Sart Tilman, Belgium
(Received 11 September 2014; revised manuscript received 27 November 2014; published 24 December 2014)

We use first-principles calculations to understand the behavior of the Seebeck coefficient (S) in Bi_2Te_3 as a function of isotropic pressure. We perform calculations up to 5 GPa using density functional theory and with thermoelectric properties extracted using Boltzmann transport equations. We find that with the increase in pressure the system becomes more metallic, in agreement with previous calculations on Sb_2Te_3. For p-type doping the overall behavior is a decrease in S with an increase in pressure. At small values of hole doping ($p = 1.8 \times 10^{18}$ cm^{-3}), we obtain an anomalous variation of S under 2 GPa, which is an indication of the electronic topological transition. For n-type doping, S slightly increases with pressure.

DOI: 10.1103/PhysRevB.90.245204 PACS number(s): 31.15.A−, 71.15.Mb, 72.20.Pa, 61.50.Ks

I. INTRODUCTION

Bismuth telluride (Bi_2Te_3) is a well-known narrow band-gap semiconductor. Over the past years this compound has been widely studied principally for its thermoelectric properties. It currently stands as one of the best room-temperature thermoelectric materials. Studies on bismuth telluride are not limited to thermoelectricity as Bi_2Te_3 has been shown to exhibit other unusual phenomena. In particular, a recent study has suggested the existence of an electronic topological transition (ETT) upon application of a 3-GPa hydrostatic pressure [1]. Intrinsically, Bi_2Te_3 is an anisotropic system that consists of weakly bonded stacks of atomic layers. Surprisingly, the ETT has been attributed to effects occurring within covalently bonded layers and not to modifications of the interlayer weaker bonding that is much more altered by pressure. This suggests a complex interaction between intra- and interlayer bondings.

A thermoelectric (TE) material is defined as a material able to transform a temperature difference into a voltage gradient and vice versa. Over the past 60 years, materials have been optimized with the aim of finding a TE material with high efficiency. This efficiency is quantified by the so-called TE figure of merit, a dimensionless parameter given by the formula,

$$ZT = \frac{S^2 \sigma T}{\kappa}, \tag{1}$$

where S is the thermopower, or Seebeck coefficient, related to the magnitude of the voltage induced in response to a gradient in temperature, σ is the electrical conductivity, T is the absolute temperature, and κ is the thermal conductivity (which is the sum of electronic and phonon thermal conductivities: $\kappa = \kappa_e + \kappa_l$). Despite the simplicity of Eq. (1), high-ZT values are not easily achieved due to the fact that high σ and low κ are usually not observed simultaneously [2]. In principle, there is no thermodynamic limitation to the increase in ZT, but only modest improvements have been achieved so far. This is due to the difficulty to increase S (or σ) while keeping low values for κ as these quantities are strongly correlated [3]. In the low-temperature regime the electronic conductivity of a metal or a semiconductor is approximately given by the relation: $\sigma \propto N(E_F)\langle v^2 \rangle \tau$, where $N(E_F)$, $\langle v \rangle$, and τ are the density of states at the Fermi energy, the average of the Fermi velocity, and the relaxation time, respectively. To obtain a significant value of σ the charge carriers should have energies away from band edges to combine large density of states (DOS) and high mobility. In the same regime the thermopower is given by $S \propto T(d\sigma/dE)/\sigma$, which raises a contradiction. To increase S, the carriers should be close to the band edge where the logarithmic derivative of the electronic conductivity with energy is large [2]. For semimetals and metals where the energy dependence of the conductivity changes slowly with temperature, $(d\sigma/dE)/\sigma$ approaches $\frac{1}{KT_F}$ where T_F is the Fermi temperature (with typical values of 10^4–10^5), which explain the low Seebeck coefficient in metals.

New state-of-the-art thermoelectric devices are tellurium-based alloys, such as p-$Bi_xSb_{2-x}Te_{3-y}Se_y$ with $x \approx 0.5$, $y \approx 0.12$, and n-$Bi_2(Se_yTe_{1-y})_3$ with $y \approx 0.05$ for a range of temperatures between 200 and 400 K [4]. Doped alloys, such as Bi_2Te_3-Sb_2Te_3 exhibit a ZT value close to 1 at room temperature. In order to compete with conventional coolers, TE materials need to reach a value of $ZT \approx 4$ corresponding to ≈30% of the Carnot efficiency [5–7]. In the mid 1990s, theoreticians suggested that thermoelectric properties could be enhanced by quantum confinement of the carriers [8,9]. On the experimental side, new materials have been synthesized that yielded higher ZT values. The most common materials are clathrates which have a large unit cell with voids [10] or skutterudites which contain corner-sharing octahedra. These tilted octahedra create large voids which can be filled by atoms, mostly rare-earth or heavy atoms, to reduce thermal conductivity [8]. Pressure tuning is another approach developed to enhance thermoelectric efficiency [7]. High pressure as well as temperature have a strong influence on the materials DOS, especially in the vicinity of the electronic gap. Since most TE materials are narrow band-gap semiconductors, this pressure dependence of the energy gap allows the optimization of TE properties. Heavily doped $Sb_{1.5}Bi_{0.5}Te_3$ shows a large increase in ZT under 2 GPa of pressure [7]. The concentration of Sb is three times larger than Bi, which suggests that the Sb_2Te_3 component of the alloy is responsible for this anomalous behavior. *Ab initio* calculations were performed on Sb_2Te_3 under nonhydrostatic pressure [11], and it was found that the Seebeck coefficient decreases with

*wibarra@ulg.ac.be

pressure, but the power factor ($S^2\sigma$) increases because the system metallizes, which increases the electrical conductivity.

In this paper, we perform *ab initio* density functional calculations for Bi_2Te_3 under pressure. We compare our results with those obtained by experiments and with theoretical results on Sb_2Te_3. Our results provide an overview of the relation between electronic and transport properties with applied pressure. Furthermore, we find that, even when the system metallizes with pressure, the Seebeck coefficient for an *n*-type semiconductor improves with pressure but only in the out-of-plane direction (along the *z* axis). These effects are observed with an indication of ETT transition.

II. TECHNICAL INFORMATION

All the calculations have been performed in the framework of density functional theory (DFT) [12,13] as implemented in the Vienna *ab initio* simulation package [14–16]. The PW91 generalized gradient approximation (GGA) was used for the exchange-correlation energy [17]. For self-consistent field (SCF) calculations the plane-wave basis expansion has been set to 300 eV, and the Monkhorst and Pack scheme [18] was used to discretize the reciprocal space with a uniform grid of $10 \times 10 \times 10$ k points in the entire Brillouin zone. We used the projector augmented-wave method including Bi semicore d orbitals within a fully relativistic scheme. This allowed us to take into account spin-orbit interactions. The structures were relaxed under pressure (estimated accuracy of 0.1 GPa), and SCF calculations have been performed to determine the charge density. To obtain the structures at any given hydrostatic pressure, we enforced the convergence of the individual components of the stress tensor (not the trace) within 0.15 GPa of the target pressure value. This request for isotropic pressure actually led to unrealistic structures when van der Waals functionals were used (abnormally large c/a values). Therefore we decided to use GGA functionals for all calculation results presented here. The electronic band structures, related DOS, and thermoelectric properties were computed in an ulterior non-SCF calculation with a $20 \times 20 \times 20$ k-point grid. The calculation of the thermoelectric properties, such as the Seebeck coefficient (S), electronic conductivity (σ), and power factor ($S^2\sigma$) were performed using Boltzmann transport equations within the constant relaxation time approximation as implemented in the BOLTZTRAP code [19]. Under this approximation, the Seebeck coefficient as a function of temperature (T) and chemical potential (μ) is given by

$$S_{ij} = (\sigma^{-1})_{\alpha i}\, \nu_{\alpha j}, \tag{2}$$

where $(\sigma^{-1})_{\alpha i}$ and $\nu_{\alpha j}$ are the transport tensors,

$$\sigma_{\alpha\beta}(T;\mu) = \frac{1}{\Omega}\int \Xi_{\alpha\beta}(\epsilon)\left[-\frac{\partial f_\mu(T;\epsilon)}{\partial\epsilon}\right]d\epsilon, \tag{3}$$

$$\nu_{\alpha\beta}(T;\mu) = \frac{1}{eT\Omega}\int \Xi_{\alpha\beta}(\epsilon)(\epsilon-\mu)\left[-\frac{\partial f_\mu(T;\epsilon)}{\partial\epsilon}\right]d\epsilon, \tag{4}$$

where $f_\mu(T;\epsilon)$, Ω, and e are the Fermi distribution, the volume of the cell, and the electronic charge, respectively. $\Xi_{\alpha\beta}(\epsilon)$ is the so-called transport distribution function, which is the energy-projected conductivity tensor defined by integrating the **k**-dependent conductivity tensor $[\sigma_{\alpha\beta}(i,\mathbf{k})]$,

$$\Xi_{\alpha\beta}(\epsilon) = \frac{1}{N}\sum_{i,\mathbf{k}}\sigma_{\alpha\beta}(i,\mathbf{k})\frac{\delta(\epsilon-\epsilon_{i,\mathbf{k}})}{d\epsilon}, \tag{5}$$

where the relaxation-time ($\tau_{i,\mathbf{k}}$) dependence is included as follows:

$$\sigma_{\alpha\beta}(i,\mathbf{k}) = e^2\tau_{i,\mathbf{k}}v\alpha(i,\mathbf{k})v\beta(i,\mathbf{k}). \tag{6}$$

$\sigma_{\alpha\beta}(i,\mathbf{k})$ is obtained by calculating energy bands on a grid of k points via the group velocities $v_\alpha(i,\mathbf{k})$, then $\Xi_{\alpha\beta}(\epsilon)$ and all the derived properties can be computed. The doping is treated within the rigid-band approximation, and the effect of temperature on these bands was neglected. BOLTZTRAP performs a Fourier expansion on the band energies taking into account the symmetry-using star functions. This allows to increase the number of points for a better representation of the electronic bands around the Fermi energy. Further details of the implementation can be found in the papers of Madsen and Singh [19] and Scheidemantel *et al.* [20].

III. STRUCTURE AND ELECTRONIC PROPERTIES UNDER PRESSURE

Bi_2Te_3 has a rhombohedral structure with space group No. 166 R-3m with three formula units per conventional cell (Fig. 1). In the nonprimitive (conventional) hexagonal cell, Te_1 is located in the 3a Wyckoff position [the (0,0,0) position in reduced coordinates for the primitive rhombohedral cell], whereas Bi and Te_2 are located at the 6c position $(\pm X_{\mathrm{Bi,Te}}, \pm X_{\mathrm{Bi,Te}}, \pm X_{\mathrm{Bi,Te}})$. In the hexagonal nonprimitive cell, the structure consists of stacked layers along the c axis with the following sequence Te_2-Bi-Te_1-Bi-Te_2. In this representation, the layered nature of the compound can be easily identified. The tellurium atoms in adjacent layers are bonded mostly by van der Waals forces. It is worth mentioning that these kinds of interactions are neglected in our calculations, but the structure nevertheless agrees with previously reported experiments [21], and this means that

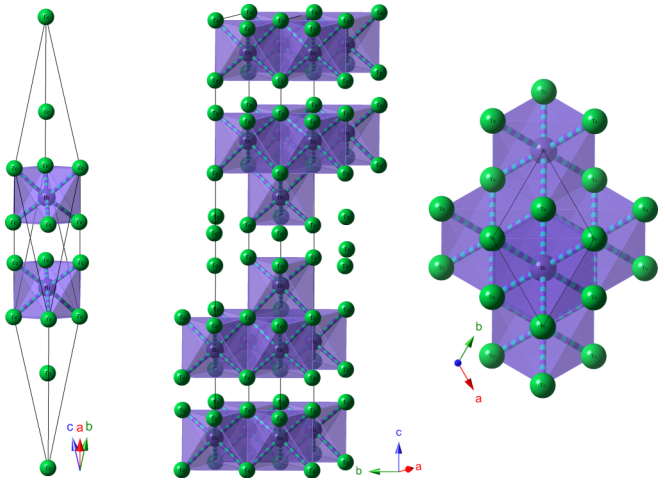

FIG. 1. (Color online) Crystal structure of Bi_2Te_3 (Bi is represented by purple balls, and Te is represented by green balls). The primitive rhombohedral cell (left) and the nonprimitive hexagonal cell (center and right) with three chemical formulas are shown.

these layers are partially bonded by covalent interactions. Hereafter we will always refer to the primitive rhombohedral cell. The calculated lattice parameter is 10.54 Å, which is 0.67% larger than the experiment, whereas the lattice angle of the rhombohedral cell is 24.48°, 1.26% larger than the experimental data. Due to the use of GGA pseudopotentials, the overestimation of the lattice parameters was expected. The optimized fractional coordinates are $X_{Bi} = \pm 0.21$ and $X_{Te} = \pm 0.400$. Both values agree with the experiment within less than 1% [21]. Because Bi is a heavy element, it is well known that its electronic band structure is strongly affected by spin-orbit interactions (SOIs) [22]. The differences that we obtained with the inclusion of SOIs were similar to those addressed in Ref. [22]. In the calculations without SOIs the band gap lies incorrectly at the Γ point with a value of 388 meV. With the inclusion of SOIs the gap becomes indirect. Due to these differences in the electronic properties, we include spin-orbit interactions in all subsequent calculations.

The conduction-band minimum lies along the Z-F high-symmetry line, and the valence-band maximum is on the a-Γ line, where a is not a high-symmetry point (this point can be found in the Brillouin zone of Larson in Ref. [22]). The obtained value of 80 meV is smaller than the 130-meV [23] experimental value at room temperature. On other hand, this gap value agrees with other theoretical papers (83 meV) [24]. However, in Ref. [24], experimental lattice parameters were used whereas in the present paper the entire structure is relaxed in order to quantify the effect of pressure on the electronic properties. Figure 2 shows the evolution of the lattice parameters, bond lengths, and volume as a function of pressure. The interlayer separation decreases with pressure: The Te-Te bond length decreases more rapidly than the Bi-Te bond length. This behavior is expected since the layers are weakly bound. In the xy plane, the structure tends to be rearranged due the enhanced proximity of the layers. Our calculations agree with experimental data on Bi_2Te_3 under hydrostatic pressure [1,25]. It was shown that hexagonal parameters a and c are constantly decreasing with pressure, the c/a ratio reaching a minimum value around 1.5 GPa [25]. In our calculations the minimum

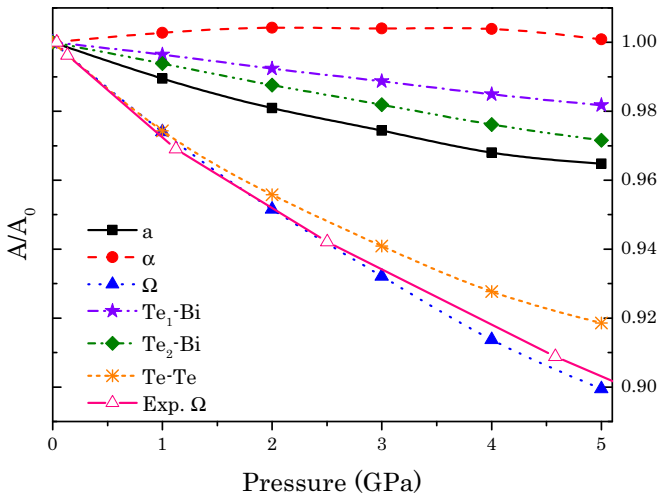

FIG. 2. (Color online) Normalized changes in lattice parameter (a), lattice angle (α), primitive cell volume (Ω), and atomic bonds for Bi_2Te_3. Experimental volume extracted from Ref. [1].

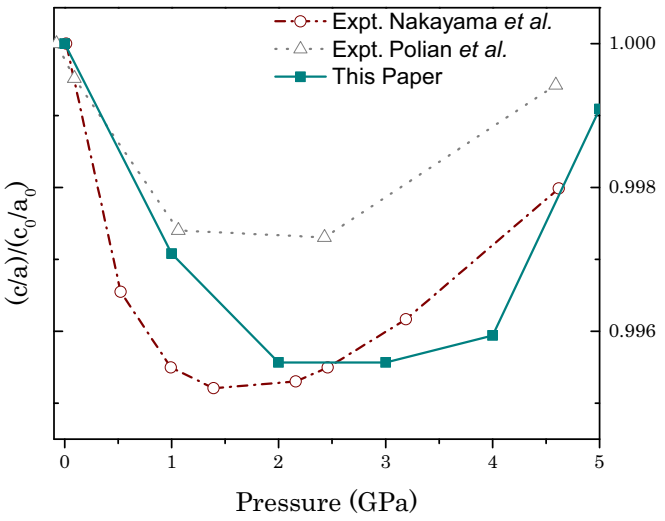

FIG. 3. (Color online) Normalized changes in the c/a ratio for the hexagonal representation of Bi_2Te_3. Experimental data were extracted from Refs. [25] (empty circles) and [1] (empty triangles).

c/a ratio lies between 2 and 3 GPa (see Fig. 3). This minimum could be related to the ETT [1], and we further investigate this point using *ab initio* calculations in what follows.

The computed bulk modulus is equal to 28.1 GPa, which deviates from the experimental value by −13.4% (32.5 GPa) [1]. The evolution of the electronic band structure under pressure is shown in Fig. 4. The lowest conduction bands shift to lower energies with the increase in pressure. At zero pressure the top of the valence band shows two quasidegenerate maxima. With the increase in pressure, the maxima on the Z-F high-symmetry line go to lower energies, and the quasidegeneracy is lifted. This is actually responsible for the ETT in Bi_2Te_3. At zero pressure the two main peaks (the one on the a-Γ line and the one on the Z-F line) contribute to the transport.

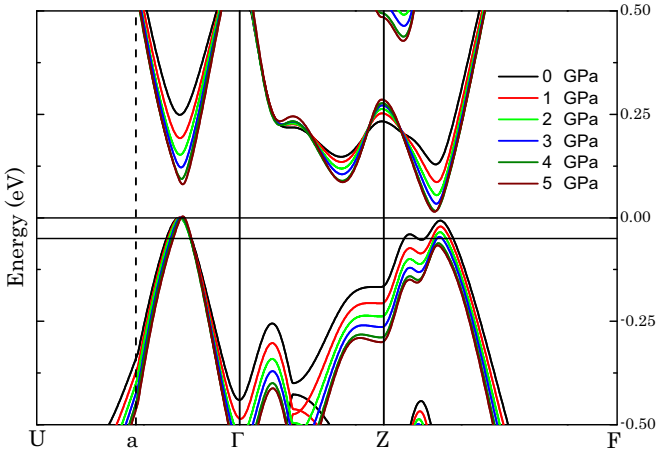

FIG. 4. (Color online) Electronic band structure of Bi_2Te_3 under pressure in steps of 1 GPa. The electronic band structure shows a constant approach between lower conduction bands. The valence-band maximum is taken as the reference energy, and the horizontal lines represent the limits of the electronic states contributing to the Fermi surfaces plotted in Fig. 9 (doping case 0 GPa).

Afterwards just the one on the a-Γ line remains. Under pressure, the Fermi level changes to maintain the carrier concentration. Even at 5 GPa no conduction band crosses the Fermi level, therefore, even though the gap is reducing, the system is not yet metallic. The constant gap reduction and the nonzero gap up to 5 GPa agree with the experiments of Vilaplana *et al.* [26]. They report a nonzero gap up to 5.5 GPa and a pressure coefficient of -6.4 meV/GPa for measures of the optical gap. Li *et al.* [27] report a pressure coefficient of -19.73 meV/GPa from resistivity measurements as a function of temperature and pressure. We determine a value of the pressure coefficient of -15 meV/GPa for the indirect gap.

IV. THERMOELECTRIC PROPERTIES

Using the electronic band structure and the related DOS, we calculate transport properties via the BOLTZTRAP code. Due to the symmetry of the system, the electronic properties are anisotropic. In order to visualize the repercussions of this anisotropy on the transport properties, we plot the transport distribution function [Eq. (5)] for in-plane and out-of-plane components at zero pressure as a function of the chemical potential (Fig. 5). For energies close to E_F (± 0.5 eV), the states which contribute in a significant way for both in-plane (xx) and out-of-plane (zz) are similar (for symmetry reasons $\Xi_{yy} = \Xi_{xx}$) but not equal. We plot Ξ for the range of values of applied pressure because as we will show hereafter the changes due to the applied pressure are also anisotropic [Fig. 7(a)].

We compute the temperature dependence of the Seebeck coefficient using the experimental carrier concentration of $p = 1.3 \times 10^{19}$ cm^{-3} obtained at room temperature and pressure in Refs. [24,28]. The properties of the electronic states in the vicinity of the gap play a dominant role in the Seebeck coefficient, but it is well known that in DFT the gap is underestimated. In Fig. 6 we have used a "scissors" operator which artificially corrects the gap value by performing a rigid shift in the conduction bands to higher energies (47-meV shift). As can be seen in the figure, this does not improve the agreement: For low T the correction is not needed,

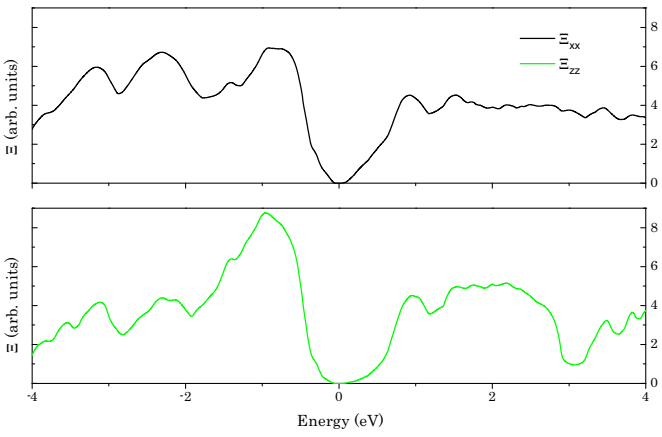

FIG. 5. (Color online) Transport distribution function for in-plane (xx) and out-of-plane (zz) of Bi_2Te_3 at zero pressure for different values of energy. Positive energies correspond to electrons and negatives to holes.

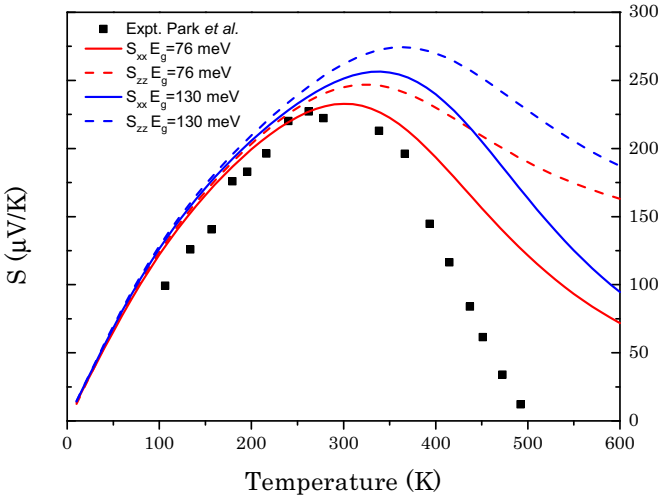

FIG. 6. (Color online) Temperature dependence of the Seebeck coefficient for a theoretical gap (red solid line S_{xx} and red dashed line S_{zz}) and for a gap [23] fixed by the scissor operator (blue solid line S_{xx} and blue dashed line S_{zz}) with a doping level of $p = 1.3 \times 10^{19}$ cm^{-3}. Black squares are the data extracted from Ref. [24].

and for higher T the gap is actually shrunk by thermal effects, yielding better agreement with the original DFT value. This compensation between DFT underestimation and thermal narrowing of band gaps is probably present in many *ab initio* thermoelectrical calculations. Figure 7 shows the (a) transport distribution function (Ξ) as a function of the chemical potential, (b) σ, (c) ν, and (d) S as a function of the carrier concentration at 300 K for different values of pressure. We find a saturation point in Ξ with the increase in pressure. There are two valence bands that contribute to the increase in the transport distribution function, but only one shifts to higher energies (closer to the Fermi energy) with the increase in pressure. This band is located on the a-Γ line. For n-type doping there is no saturation with pressure because as more bands approach the Fermi level, the transport distribution function is enhanced. The lower conduction band in the Z-F high-symmetry line becomes narrower. The Z-F trajectory is almost completely in plane, and for this reason σ_{xx} grows faster than σ_{zz}.

In the literature a value of electrical resistivity at room temperature and pressure is $\approx 1.43 \times 10^{-5}\ \Omega$ m [21]. Using this value, we estimate the relaxation time $\tau = 1.0 \times 10^{-14}$ s and use this value for the electrical conductivity and for the parameter ν [in the Seebeck coefficient it is not necessary as it cancels out of Eq. (2)]. The general dependence of σ with doping is the following: With the increase in doping, no matter the type of carrier, the chemical potential shifts towards energy values where the DOS increases as does the electrical conductivity. With pressure, bands above and below the Fermi level move towards it, which increases the density of states around the Fermi level, and σ increases. For what concerns the electrical conductivity, the integration of the derivative of the Fermi function and transport distribution function guarantee positive values. In ν (and therefore the Seebeck coefficient) the same function is multiplied by $(\epsilon - \mu)$, which is an odd function. For this reason, values of positive and negative

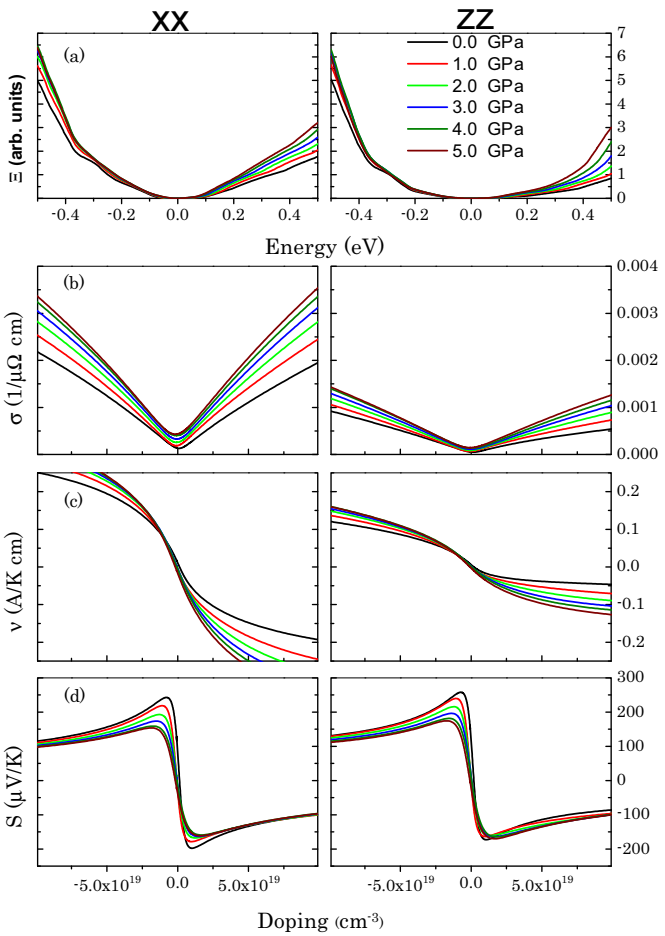

FIG. 7. (Color online) From top to bottom: The transport distribution function with respect to the energy where positive values correspond to an n type of doping and a p type for negative values. The electronic conductivity, ν, and Seebeck coefficient are plot with respect to the carrier concentration (positive values correspond to electrons and negative for holes). All the plots show in-plane (left) and out-of-plane (right) values.

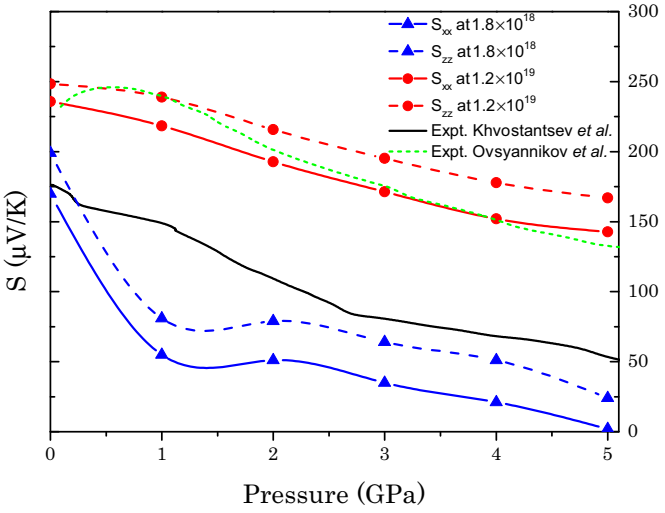

FIG. 8. (Color online) Pressure dependence of the in-plane (solid line) and out-of-plane (dashed line) Seebeck coefficients at 300 K. Green dotted and black solid lines are experimental data extracted from Refs. [30,31].

chemical potentials (electron or hole dopings) can cancel out each other [see Figs. 7(c) and 7(d)].

In the Seebeck coefficient graph for hole doping we can see that, for both (xx) and (zz) components, the maximum value is reached at relatively small doping. This maximum decays regularly with pressure, and the carrier density at which this maximum occurs shifts to higher concentrations. The graphs of ν and σ show that both increase with pressure, but the increase in ν is smoother than the increase in σ. Therefore, the multiplication of Eq. (2) gives a decrease in the Seebeck coefficient with an increase in P. For the case of n-type Bi_2Te_3 at low doping (up to $n = 2.5 \times 10^{19}$ cm^{-3}), the overall behavior is the same as for hole doping. Above this doping value we distinguish two cases. For the in-plane Seebeck, the increase in the value of ν with pressure is compensated by the increase in the electrical conductivity, and the variation in S_{xx} with pressure is negligible. In the case of the out-of-plane Seebeck, the electrical conductivity increases with pressure but not enough to balance the increase in ν, which gives a small improvement of S_{zz} with pressure.

Figure 7 shows the overall behavior of the thermoelectric properties of Bi_2Te_3 and their relation to carrier concentration and pressure. So far the analysis is insufficient to explain the improvement of the Seebeck coefficient with pressure found experimentally [29,30] .The main reason is that the experimental carrier concentrations are too low compared with the scale used in Fig. 7. In the paper of Khvostantsev *et al.* [30] the samples had carrier concentrations of $p = 1.2 \times 10^{19}$ cm^{-3} for the p type and $n = 1.1 \times 10^{19}$ cm^{-3} for the n type of doping at room temperature up to 9 GPa. In a recent experimental paper [31], the carrier concentration is not mentioned, but the Seebeck coefficient suggests a similar order of magnitude. Figure 8 shows our results and the extracted experimental data at 300 K [30,31]. The experimental carrier concentration reported in Ref. [30] was used and shows good agreement between our calculations and the experiment (see Fig. 6). We compare our values of S with those in Ref. [31] at zero pressure, and we fix the doping level at $p = 1.8 \times 10^{18}$ cm^{-3} to match the experimental data, assuming that the experiment was performed at room temperature. Our results agree very well with the experiments, especially with those with high carrier concentrations. For those values with small doping levels, larger discrepancies are expected due to the vicinity to the Fermi level and our small band gap. The agreement with experiment even at small values of carrier concentration is nevertheless reasonable. However, although we reproduce the trends very well, we do not observe any improvement in S close to 1 GPa, contrary to Ref. [30]. This disagreement could arise from the fact that we are neglecting van der Waals interactions which could be relevant for details of the electronic structure, and therefore, the transport properties. Thermal expansion is also neglected, but we assume that its effects would be small as both our calculations and the mentioned experiments were carried out close to room temperature and the cell and internal parameters agree well. The shoulder at 2 GPa could eventually

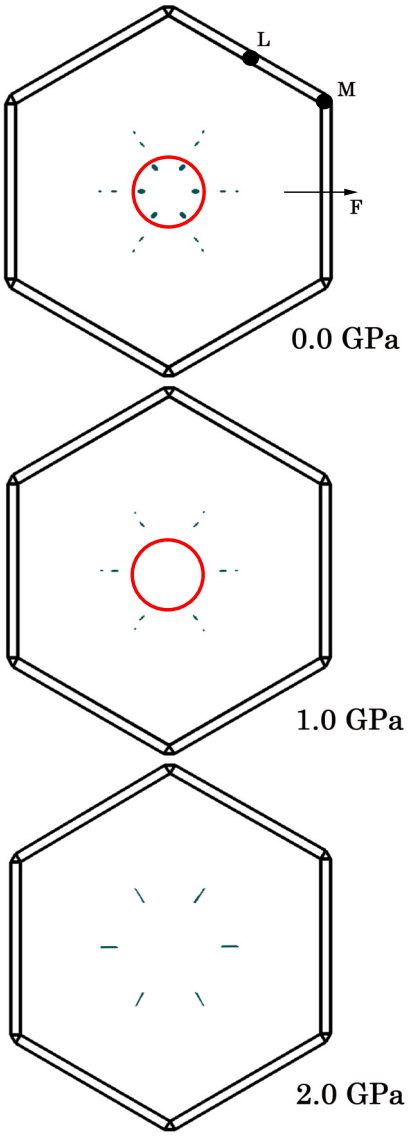

FIG. 9. (Color online) View of the (1 1 1) plane of the Brillouin zone. The small pockets represent available electronic states close to the top of the valence band (see Fig. 4). At 1 GPa the top of the valence band located on the Z-F lines disappears. Red circles encompass the corresponding electron pockets that vanish with the ETT. Above 2 GPa the Fermi surfaces do not evolve anymore.

be explained by an ETT that was reported to occur between 3 and 4 GPa (we assume an accuracy of ±1 GPa). Polian and co-workers [1] plot the Birch-Murnaghan's equation of states (BM-EOS) linearization versus the Eulerian strain. In the absence of transition this strain should be linear with respect to the BM-EOS. They found that at 3.2 GPa the linearization of the strain breaks down, which leads them to assume the existence of an ETT transition [1]. The effect of the ETT is only present in plane whereas out of plane it is completely absent. Our results show that, if this shoulder arises from an ETT, it would be reflected in both in-plane and out-of-plane transport properties. Moreover, the effects of the ETT disappear when the system is highly doped. We plot the Fermi surfaces, assuming zero temperature, as a function of pressure (Fig. 9). The Fermi level was fixed by imposing the hole concentration value $p = 1.8 \times 10^{18}$ cm^{-3} for 0–2 GPa. The largest change with pressure happens between 0 and 1 GPa. At zero pressure, the system has two quasidegenerate maxima on the valence band, one in the a-Γ direction and the other in the Z-F direction. The difference in energy between these two maxima at zero pressure is 7 meV and reaches 21.5 meV at 1 GPa. With the increase in pressure the top of the valence band positioned in the Z-F high-symmetry line shifts to lower energies. At $p = 1.8 \times 10^{18}$ cm^{-3} and 1 GPa of hydrostatic pressure, this maximum gets lower than E_F, and the corresponding pockets disappear from the Fermi surface (see Fig. 9), which is characteristic of an ETT. One can notice in Fig. 9 that the distinctive pockets present at 1 GPa have merged at 2 GPa. This is actually responsible for the shoulder observed in the Seebeck coefficient in this pressure range.

V. CONCLUSION

We have performed *ab initio* calculations of the structural and thermoelectric properties of Bi_2Te_3 under hydrostatic pressure up to 5 GPa. We find that the gap decreases with pressure, inducing more metallicity and that the value of S decreases constantly with pressure as computed previously for the Sb_2Te_3 system [11]. The pressure dependence of the Seebeck coefficient is in qualitative agreement with available data, however the peak found experimentally at 1 GPa is not reproduced [30]. For the case of n-type doping, the application of pressure leads to a moderate improvement of the Seebeck coefficient. This is again comparable to what was obtained for Sb_2Te_3. However, experimental studies on Bi_2Te_3 doped with electrons do not find the enhancement in S found here [32]. This could be explained by the fact that only the out-of-plane Seebeck coefficient increases whereas the in-plane Seebeck coefficient shows a constant decrease with pressure. We suggest that the discrepancy between the experiments in Ref. [32] and our theoretical results could be due to the fact that the experiments were performed on powders subject to preferential orientation under pressure and to differences in carrier concentrations. We point out that the enhancement of the Seebeck shown here is limited to highly doped systems (above $n = 2.5 \times 10^{19}$ cm^{-3}), whereas the experimental carrier concentration in Ref. [30] is only $n = 1.1 \times 10^{19}$ cm^{-3}. Similarities between our results and those obtained for Sb_2Te_3 suggest two things that have not been addressed up to now. First, the evolution of the electronic bands with pressure that we describe here should be present in Sb_2Te_3 and second, the thermoelectric properties of Bi_2Te_3 should be enhanced with uniaxial strain. In particular, the behavior of the electronic bands for Sb_2Te_3 under hydrostatic pressure could be an interesting topic as, according to Ref. [11], this system has three quasidegenerate maxima on the valence band instead of the two that exist in Bi_2Te_3.

Our calculations indicate a minimum in the c/a ratio at 2 GPa, which agrees with experiments that report the minimum around 1.5 GPa [1,25]. We have shown that at this pressure and with a low carrier concentration the evolution of the Fermi surface is characteristic of an ETT transition. The ETT is actually caused by the nonlinear band-structure effects that occur when pressure is applied to an intrinsically anisotropic semiconductor compound, such as Bi_2Te_3.

ACKNOWLEDGMENTS

The authors acknowledge an A.R.C. grant (Grant No. TheMoTherm 10/15-03) from the Communauté Française de Belgique. Computer time was made available by the Belgian CECI, SEGI-ULg, and PRACE projects NanoTherm (Project No. 2IP FP7 RI-283493) and ThermoSpin on ARCHER (Project No. 3IP FP7 RI-312763).

[1] A. Polian, M. Gauthier, S. M. Souza, D. M. Trichês, J. Cardoso de Lima, and T. A. Grandi, Phys. Rev. B **83**, 113106 (2011).
[2] D. Parker, X. Chen, and D. J. Singh, Phys. Rev. Lett. **110**, 146601 (2013).
[3] S. Tang and M. S. Dresselhaus, arXiv:1406.1842.
[4] R. Venkatasubramanian, E. Siivola, T. Colpitts, and B. O'Quinn, Nature (London) **413**, 597 (2001).
[5] F. J. DiSalvo, Science **285**, 703 (1999).
[6] A. Majumdar, Science **303**, 777 (2004).
[7] D. A. Polvani, J. F. Meng, N. V. Chandra Shekar, J. Sharp, and J. V. Badding, Chem. Mater. **13**, 2068 (2001).
[8] G. J. Snyder and E. S. Toberer, Nature Mater. **7**, 105 (2008).
[9] L. D. Hicks and M. S. Dresselhaus, Phys. Rev. B **47**, 12727 (1993).
[10] G. S. Nolas, J. Poon, and M. Kanatzidis, MRS Bull. **31**, 199 (2006).
[11] T. Thonhauser, T. J. Scheidemantel, J. O. Sofo, J. V. Badding, and G. D. Mahan, Phys. Rev. B **68**, 085201 (2003).
[12] P. Hohenberg and W. Kohn, Phys. Rev. **136**, B864 (1964).
[13] W. Kohn and L. J. Sham, Phys. Rev. **140**, A1133 (1965).
[14] G. Kresse and J. Hafner, Phys. Rev. B **47**, 558 (1993).
[15] G. Kresse and J. Hafner, Phys. Rev. B **49**, 14251 (1994).
[16] G. Kresse and J. Furthmüller, Phys. Rev. B **54**, 11169 (1996).
[17] J. P. Perdew, J. A. Chevary, S. H. Vosko, K. A. Jackson, M. R. Pederson, D. J. Singh, and C. Fiolhais, Phys. Rev. B **46**, 6671 (1992).
[18] H. J. Monkhorst and J. D. Pack, Phys. Rev. B **13**, 5188 (1976).
[19] G. K. H. Madsen and D. J. Singh, Comput. Phys. Commun. **175**, 67 (2006).
[20] T. J. Scheidemantel, C. Ambrosch-Draxl, T. Thonhauser, J. V. Badding, and J. O. Sofo, Phys. Rev. B **68**, 125210 (2003).
[21] P. D. O. Madelung, *Semiconductors: Data Handbook*, 3rd ed. (Springer-Verlag, Berlin/Heidelberg, 2004).
[22] P. Larson, Phys. Rev. B **68**, 155121 (2003).
[23] I. G. Austin, Proc. Phys. Soc. **72**, 545 (1958).
[24] M. S. Park, J.-H. Song, J. E. Medvedeva, M. Kim, I. G. Kim, and A. J. Freeman, Phys. Rev. B **81**, 155211 (2010).
[25] A. Nakayama, M. Einaga, Y. Tanabe, S. Nakano, F. Ishikawa, and Y. Yamada, High Press. Res. **29**, 245 (2009).
[26] R. Vilaplana, O. Gomis, F. J. Manjón, A. Segura, E. Pérez-González, P. Rodríguez-Hernández, A. Muñoz, J. González, V. Marín-Borrás, V. Muñoz Sanjosé *et al.*, Phys. Rev. B **84**, 104112 (2011).
[27] C.-Y. Li, A. L. Ruoff, and C. W. Spencer, J. Appl. Phys. **32**, 1733 (1961).
[28] H. Kaibe, Y. Tanaka, M. Sakata, and I. Nishida, J. Phys. Chem. Solids **50**, 945 (1989).
[29] S. V. Ovsyannikov, V. V. Shchennikov, G. V. Vorontsov, A. Y. Manakov, A. Y. Likhacheva, and V. A. Kulbachinskii, J. Appl. Phys. **104**, 053713 (2008).
[30] L. G. Khvostantsev, A. I. Orlov, N. K. Abrikosov, T. E. Svechnikova, and S. N. Chizhevskaya, Phys. Status Solidi A **71**, 49 (1982).
[31] S. Ovsyannikov, Y. Grigoreva, G. Vorontsov, L. Lukyanova, V. Kutasov, and V. Shchennikov, Phys. Solid State **54**, 261 (2012).
[32] M. Jacobsen, S. Sinogeikin, R. Kumar, and A. Cornelius, J. Phys. Chem. Solids **73**, 1154 (2012).